

A wave equation migration method for receiver function imaging: 2. Application to the Japan subduction zone

Ling Chen

Seismological Laboratory, Institute of Geology and Geophysics, Chinese Academy of Sciences, Beijing, China

Lianxing Wen

Department of Geosciences, State University of New York at Stony Brook, Stony Brook, New York, USA

Tianyu Zheng

Seismological Laboratory, Institute of Geology and Geophysics, Chinese Academy of Sciences, Beijing, China

Received 2 February 2005; revised 14 July 2005; accepted 19 August 2005; published 23 November 2005.

[1] The newly developed wave equation poststack depth migration method for receiver function imaging is applied to study the subsurface structures of the Japan subduction zone using the Fundamental Research on Earthquakes and Earth's Interior Anomalies (FREESIA) broadband data. Three profiles are chosen in the subsurface imaging, two in northeast (NE) Japan to study the subducting Pacific plate and one in southwest (SW) Japan to study the Philippine Sea plate. The descending Pacific plate in NE Japan is well imaged within a depth range of 50–150 km. The slab image exhibits a little more steeply dipping angle ($\sim 32^\circ$) in the south than in the north ($\sim 27^\circ$), although the general characteristics between the two profiles in NE Japan are similar. The imaged Philippine Sea plate in eastern SW Japan, in contrast, exhibits a much shallower subduction angle ($\sim 19^\circ$) and is only identifiable at the uppermost depths of no more than 60 km. Synthetic tests indicate that the top 150 km of the migrated images of the Pacific plate is well resolved by our seismic data, but the resolution of deep part of the slab images becomes poor due to the limited data coverage. Synthetic tests also suggest that the breakdown of the Philippine Sea plate at shallow depths reflects the real structural features of the subduction zone, rather than caused by insufficient coverage of data. Comparative studies on both synthetics and real data images show the possibility of retrieval of fine-scale structures from high-frequency contributions if high-frequency noise can be effectively suppressed and a small bin size can be used in future studies. The derived slab geometry and image feature also appear to have relatively weak dependence on overlying velocity structure. The observed seismicity in the region confirms the geometries inferred from the migrated images for both subducting plates. Moreover, the deep extent of the Pacific plate image and the shallow breakdown of the Philippine Sea plate image are observed to correlate well with the depth extent of the seismicity beneath NE and SW Japan. Such a correlation supports the inference that the specific appearance of slabs and intermediate-depth earthquakes are a consequence of temperature-dependent dehydration induced metamorphism occurring in the hydrated descending oceanic crust.

Citation: Chen, L., L. Wen, and T. Zheng (2005), A wave equation migration method for receiver function imaging: 2. Application to the Japan subduction zone, *J. Geophys. Res.*, *110*, B11310, doi:10.1029/2005JB003666.

1. Introduction

[2] The receiver function method has been extensively adopted in the studies on the crustal and upper mantle discontinuities [e.g., Langston, 1977; Vinnik, 1977; Owens *et al.*, 1987; Sheehan *et al.*, 1995; Dueker and Sheehan, 1997; Li *et al.*, 2000; Zhu, 2000; Ai *et al.*, 2003; Gilbert *et al.*, 2003; Shiomi *et al.*, 2004].

Facilitated by continuously increased number and quality of broadband seismic recordings, several migration techniques, which were mostly used in exploration seismology, have been introduced in receiver function imaging of the Earth's deep structures [Sheehan *et al.*, 2000; Ryberg and Weber, 2000; Bostock and Rondenay, 1999; Bostock *et al.*, 2001; Rondenay *et al.*, 2001; Shragge *et al.*, 2001; Poppeliers and Pavlis, 2003a, 2003b]. In the companion paper [Chen *et al.*, 2005], we develop the theoretical foundation of a wave-equation-based poststack

depth migration technique using teleseismic receiver functions. With a frequency–wave number domain one-way phase screen propagator for wave field extrapolation, the migration scheme naturally takes into account the effects of diffraction, scattering, and travel time alternation caused by lateral heterogeneities and therefore is particularly useful for imaging complex structures. Synthetic experiments demonstrate the validity and potential of the method for imaging various types of laterally heterogeneous models [Chen *et al.*, 2005]. The focus of this paper is placed on the applications of the technique to real data.

[3] We choose the Japan arc region for receiver function imaging for several reasons.

[4] 1. The Japan arc region is well known for its structural complexity associated with active subduction and collisions among four lithospheric plates [Ishida, 1989; Seno *et al.*, 1993, 1996]. The old Pacific plate subducts from east beneath the North America and Eurasian plates in NE Japan at a rate of >100 mm/yr. The relatively young Philippine Sea plate descends from south beneath the Eurasian plate in SW Japan at a convergence rate of ~45 mm/yr.

[5] 2. Japan islands are densely covered by seismic station networks (e.g., Fundamental Research on Earthquakes and Earth's Interior Anomalies (FREESIA) broadband seismograph network, Japan university network, etc.).

[6] 3. The region has high seismicity that is clearly related to the descending plates [Ishida, 1992; Umino *et al.*, 1995; Goto *et al.*, 2001; Baba *et al.*, 2002; Nakanishi *et al.*, 2002; Nakamura *et al.*, 1997; Matsumura, 1997], and the subsurface structures of both the overriding plate and the descending slabs have been extensively investigated, making it easy to study the relationships between our migrated images and the seismicity and to compare our results to the others. For example, *P* and *S* wave tomographic images show a 80- to 90-km-thick high-velocity Pacific plate dipping steeply at an angle of ~30° beneath NE Japan with sharp velocity boundaries at both the top and bottom of the slab [Zhao *et al.*, 1992b, 1994, 1997]. Using reflected or converted waves at the upper or lower boundary of the slab, a more detailed two-layer slab structure has been established, showing a thin (<10 km) low-velocity layer and a thick high-velocity lower layer, representing the subducting oceanic crust and mantle, respectively [Hasegawa *et al.*, 1978; Matsuzawa *et al.*, 1986, 1990; Umino and Hasegawa, 1993]. Some efforts have also been made to locate the upper boundary of the descending Philippine Sea plate beneath SW Japan by using reflected or converted seismic waves [e.g., Nakanishi, 1980; Nakanishi *et al.*, 1981; Iidaka *et al.*, 1990].

[7] Here we apply the new wave equation based receiver function migration method to image the subsurface structures in NE and SW Japan. Receiver function method has been recently applied to study the crustal and upper mantle structure of the Japan subduction zone [Li *et al.*, 2000; Shiomi *et al.*, 2004]. These studies either mainly focused on large-scale features of the upper mantle transition zone [Li *et al.*, 2000] or limited their studies to the upper 60 km structure of a small area in SW Japan [Shiomi *et al.*, 2004]. Coherent receiver function images of the Pacific plate and the Philippine Sea plate beneath the Japan islands have not been constructed yet. More importantly, both authors utilized stacking based techniques to process the teleseismic receiver functions. As having been pointed out in previous

receiver function studies [Sheehan *et al.*, 2000; Ryberg and Weber, 2000] and our companion paper [Chen *et al.*, 2005], complex or strong laterally heterogeneous structures may not be well imaged by stacking of receiver functions alone. Considering the complexity of the regional structures in the Japan subduction zone, migration techniques are necessary for more reliably retrieving the structural features. The purpose of this study is twofold. One is to investigate the performance of our migration method on real data sets, especially for the special structures of the descending slabs. The other is to gain a better understanding of the relationship between the slab images and seismicity. We present the seismic data and constructed receiver functions in section 2. In section 3, we show resultant migrated images for the Pacific plate and the Philippine Sea plate beneath the Japan arc. Through forward synthetic modeling, in section 4, we investigate the resolution of the migrated images in the context of data coverage, frequency content, and lateral variation of seismic velocity. In section 5, we discuss the relationships between the slab images and seismicity.

2. Seismic Data and Receiver Function Construction

[8] Teleseismic waveform data recorded at 44 nationwide FREESIA broadband stations (Figure 1) established by the National Research Institute for Earth Science and Disaster Prevention (NIED) of Japan are used in this study. 185 events occurring during a nearly 6-year period (from January of 1995 to September of 2000) with epicentral distance between 28° and 92° are selected, resulting in a total of 4170 three-component seismograms. Waveforms are windowed with a time duration of 120 s starting from 20 s before the onset of *P* wave, and receiver functions are constructed through time domain maximum entropy deconvolution of the vertical components from the radial [Wu and Zeng, 1998]. A 2.5 Hz Gaussian parameter and a water level of 0.0001 are used in the deconvolution. To eliminate high-frequency noise, receiver functions are band-pass filtered with corner frequencies from 0.03 Hz to 1 Hz. After careful visual inspection, a total of 2138 receiver functions with high signal-to-noise ratios (SNR) are selected for further processing. The one-dimensional (1-D) Preliminary Earth Reference Model (PREM) [Dziewonski and Anderson, 1981] is used to calculate the delay times of the *P*-to-*S* converted phases relative to the direct *P* wave and the piercing points of the conversions at the discontinuities. All the receiver functions are then moveout corrected to the case of horizontal slowness $p = 0$. Figure 2 shows examples of the resultant receiver functions at stations YMZ and KIS (red triangles in Figure 1) sorted by the longitude of the piercing points at 90 and 50 km depths, respectively. In both receiver function sections, an inclined converted phase is coherently detected. This converted phase likely represents the upper boundaries of the high-velocity subducting slabs.

3. Migrated Receiver Function Images of the Japan Subduction Zone

[9] According to the coverage of piercing points at depth (e.g., those at 110 and 210 km depths shown as yellow and blue points in Figure 1), we select three block areas in the

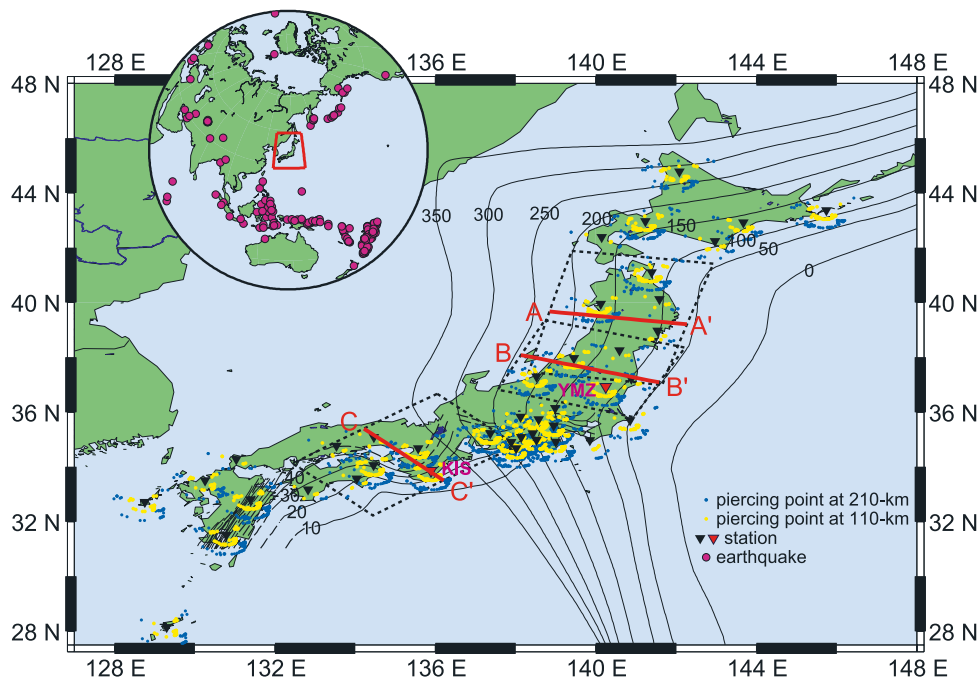


Figure 1. Japan subduction zone, seismic sampling, and three cross-sectional profiles (red lines A-A', B-B', and C-C') whose migrated images are presented in Figures 3, 4, and 5, respectively. Map inset shows the location of the study area in the northwest Pacific region. Receiver functions are obtained from the seismic data recorded at the 44 FREESIA broadband stations in Japan (inverted triangles) for 185 teleseismic events (purple circles). Piercing points at 110 and 210 km depths for *P*-to-*S* converted phases are shown as yellow and blue dots, respectively. Depth contour lines of the subducting Pacific plate are from *Gudmundsson and Sambridge* [1998], and those of the Philippine Sea plate are after *Wang et al.* [2004]. The rectangles mark the areas where the receiver functions are stacked for the three profiles.

Japan arc for subsurface structure imaging, two for NE and one for SW Japan (Figure 1). The shapes and sizes of the selected blocks are determined according to the geometry of the subducting slabs derived from the seismicity and data coverage. The blocks are designed so that their central lines (red lines A-A', B-B', and C-C' in Figure 1) are approximately perpendicular to the strikes of the descending slabs. The old Pacific plate subducts beneath NE Japan with a change of surface geometry around 38°N, as indicated by the seismicity pattern [*Umino*, 1988]. The strike of the slab is NNE in the north and becomes NE in the south. The two image blocks in NE Japan are thus designed accordingly with slightly different trending directions (Figure 1). Most parts of the northern and southern blocks (profiles A-A' and B-B') are located to the north and the south of 38°N, with a partial overlap in the middle. Distinct seismicity, volcanism and heat flow have been documented in SW Japan [*Watanabe et al.*, 1977; *Nakanishi*, 1980; *Peacock and Wang*, 1999; *Zhao et al.*, 2002]. The designed block for profile C-C' contains an area where no active volcano exists and both the heat flow and geothermal gradient are lower than the ambient region [*Yuhara*, 1973; *Okubo et al.*, 1989]. The profile trends NE-SW across the Kii Peninsula at the middle of the Nankai margin, approximately in the same location as those investigated by *Hacker et al.* [2003b] and *Yamasaki and Seno* [2003] in their studies on the thermal structure of the subduction zone. The block lengths perpendicular to the profiles are set to be large enough to ensure

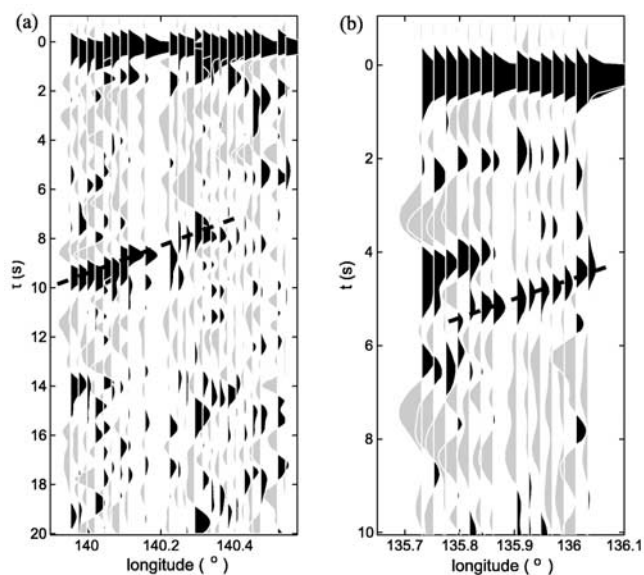


Figure 2. Moveout-corrected receiver functions (0.03–1.0 Hz) at stations (a) YMZ and (b) KIS (see Figure 1 for station locations), sorted by the longitude of the piercing points at 90 km depth for Figure 2a and 50 km depth for Figure 2b. Dashed lines mark the *P*-to-*S* converted phases of the subducting Pacific plate and Philippine Sea plate.

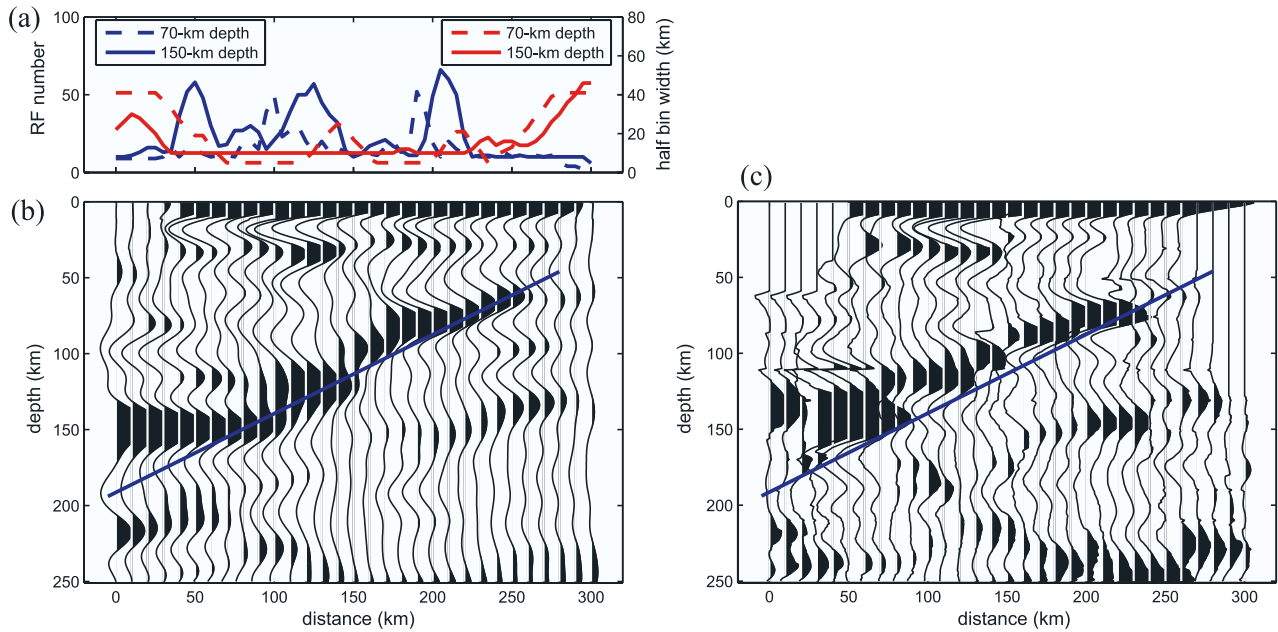


Figure 3. Receiver function images, data distribution, and stacking bin information for profile A-A' (from left to right). (a) Numbers of receiver function in the bins (blue traces) and bin widths (red traces) used in the CCP stacking at two specified depths; (b) poststack-migrated image; and (c) CCP depth image constructed from receiver functions with a frequency range of 0.03–0.3 Hz. Estimated subducting oceanic Moho from the migrated image is marked as a blue line.

that a sufficient number of receiver functions are involved in the later stacking and migration.

[10] Following the migration procedure described in our first paper [Chen *et al.*, 2005], the receiver functions are processed with time domain common conversion point (CCP) stacking and subsequent poststack depth migration. Rectangular bins are used during the CCP stacking process. The bin length, i.e., the block length, is kept unchanged along each profile. The bin width parallel to the profile is allowed to vary with the data coverage to enhance small-scale features in densely sampled areas and to construct continuous structural image for areas where data are sparse. The minimum receiver function number in each bin is determined empirically, and is set to be 10 in all cases. The receiver function numbers and bin widths at specified depths vary along all the three profiles (Figure 3a for profile A-A'; Figure 4a for profile B-B'; and Figure 5a for profile C-C'). The migrated images are obtained by adopting PREM as the 1-D migration velocity model (based on equation (13) of Chen *et al.* [2005]) and superposing the migrated contents in a chosen frequency band of 0.03–0.5 Hz for profile C-C' in SW Japan (Figure 5b) and 0.03–0.3 Hz for profiles A-A' (Figure 3b) and B-B' (Figure 4b). The CCP depth images of the same frequency contents constructed based on the method proposed by Zhu [2000] are also plotted alongside the migrated images in Figures 3c–5c.

3.1. NE Japan

[11] Along profile A-A', a strong conversion phase is clearly observed at a depth range of 50–150 km in the constructed image (Figure 3b). The converted phase has a clear near east-west inclination and a positive polarity which would indicate a conversion from a discontinuity changing from high velocity to low velocity. We interpret the phase as

the conversion from the Moho of the subducting Pacific slab. The slab image exhibits a dipping angle of $\sim 27^\circ$ to 150 km depth and becomes invisible at large depths. A horizontal phase can be seen around 25–35 km depths, marking the Moho of the overriding Eurasian plate. At ~ 150 km depth, another strong horizontal phase, possibly representing the *PpPs* Moho multiple of the overriding plate, is also visible on the continental side of the mantle (Figure 3b). The image of the subducting slab for profile B-B' appears similar as in profile A-A', except that there are some signals at larger depths that may be associated with the conversions from the slab (>150 km, Figure 4b). This is due to the fact that an adequate number of receiver functions and small bin sizes can be used in the CCP stacking at large depths (Figure 4a). The dip angle of the slab along this profile is estimated to be about 32° , several degrees greater than that of profile A-A'. In contrast to profile A-A', the Moho conversion of the overriding plate cannot be continuously traced for profile B-B', although the *PpPs* Moho multiples appear similar between the two profiles. There are strong signals around 220 to 270 km depths (Figures 4b and 4c). Their strength appears varying along the profile and their slowness is different from that of slab multiples. We interpret them as conversions from a discontinuity or discontinuities around 220–270 km depths.

[12] Compared with the migrated images, the descending slab images in the CCP depth images (Figures 3c and 4c) exhibit a shallower apparent dipping angle. This is typical that, for dipping structures, the CCP depth imaging produces images with an apparent angle shallower than their actual dipping angle, even in an ideal case with sufficiently dense data and no noise contamination (see also examples in Figures 4a and 4e of Chen *et al.* [2005]). The CCP depth images also show incoherent and, in some places, distorted

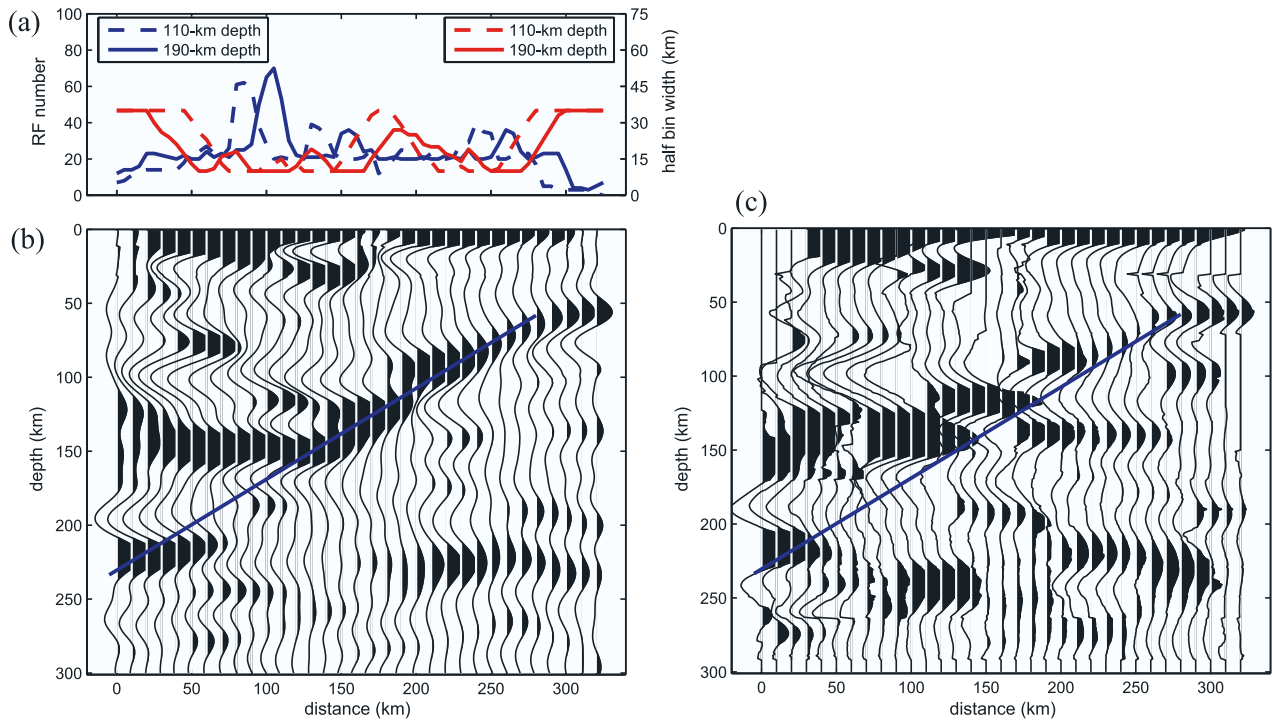


Figure 4. Same as Figure 3 except for profile B-B' (from left to right).

slab images, and many artifacts. The artifacts are particularly apparent below the slab image in profile B-B' (Figure 4c). This is probably because the multiples produced by the dipping slab are not effectively suppressed by the stacking scheme alone and significantly contaminate the image. In contrast, the migration procedure produces more coherent slab images with higher SNR, as a consequence of proper handling of the propagation effects of lateral heterogeneities through wave field extrapolation [Chen *et al.*, 2005; Sheehan

et al., 2000; Ryberg and Weber, 2000]. Comparison of the images produced by these techniques once again demonstrates the limitation of the CCP stacking techniques and the advantages of the migration method in imaging complex subsurface structures.

3.2. SW Japan

[13] In the migrated image of profile C-C' (Figure 5b), a coherent phase with a northwestward inclination is clearly

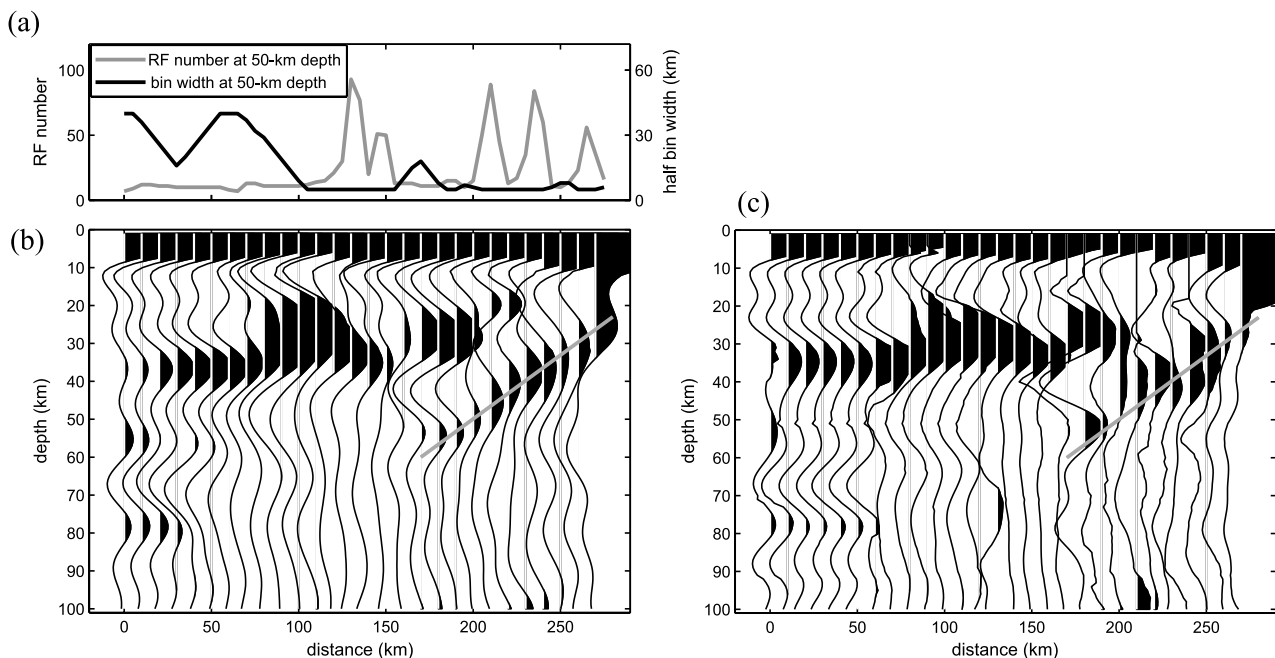


Figure 5. Same as Figure 3, except for profile C-C' (from left to right) and the migrated image (Figure 5b) and CCP depth image (Figure 5c) are constructed using frequencies from 0.03 to 0.5 Hz.

observed at the southeastern part of the profile, marking the Moho of the descending Philippine Sea plate beneath this region. The slab extends from ~ 25 km depth down to ~ 60 km but can hardly be traced further deeper. The dip angle of the slab is estimated to be about 19° in the depth range of 30–60 km. In addition to the subducting Philippine Sea plate, the Moho of the overriding plate is also visible in the migrated image with an average depth of 32 km (Figure 5b). The CCP depth image (Figure 5c) resembles the migrated image in this case because of the small dipping angle of the structure, although the dipping structure appears more coherent in the migrated image (Figure 5b).

4. Resolution of the Migrated Images Based on Synthetic Modeling

[14] As we mention in our companion paper [Chen *et al.*, 2005], the migrated images would be affected by many factors, such as, the spatial data coverage, frequency content of the receiver functions, noise, and lateral seismic heterogeneities. The influence of these factors obviously depends on the actual data condition and the geological settings in the study area. The spatial distribution of the seismic stations limits most of the data sampling beneath the land area of the Japan arc (Figure 1), making it impossible to image the subducting slabs at both shallower (<50 km in NE Japan and <30 km in SW Japan) and greater depths (>230 km in NE Japan). Even along the profiles, the data coverage is highly nonuniform (Figures 3a–5a). We thus expect that the image quality would vary within each profile. For instance, smaller bin sizes in the most part of profiles A–A' and B–B' and the southern part of profile C–C', may have resulted in correctly retrieved small-scale structural features of the slabs there, whereas enlarged bin sizes in areas of less data available unavoidably give rise to smoothed/deteriorated images at the edges of the profiles, and even in some middle segments of the images of the steeply descending Pacific plate (Figures 3–5).

[15] Perhaps, the best way to evaluate the resolution of the migrated images is through forward synthetic modeling based on the actual data coverage and other information available in the region. In this section, we discuss the resolution of the migrated images in the context of data coverage, frequency content and lateral variation of seismic velocity. As profiles A–A' and B–B' are similar, only profiles B–B' and C–C' are discussed. In the synthetic modeling, we construct subduction zone models for profiles B–B' and C–C', calculate synthetic seismograms for each model by a 2-D hybrid method [Wen and Helmberger, 1998], and construct the migrated images for the synthetics and compare them to the real data images. We discuss the effects of using different frequency contents and the influence of lateral variation of seismic velocity on the migrated images, taking profile B–B' as an example.

4.1. Image Resolution Based on Data Density and Spatial Distribution

[16] Our subduction zone model for profile B–B' is constructed based on both the structures retrieved for the profile (Figure 4b) and prior knowledge about the slab configuration in NE Japan. The model contains a high-velocity oceanic plate descending at a dip angle of 10° – 25°

at 30–50 km depth and 30° below 60 km depth. According to the previous seismic observations [Umino and Hasegawa, 1993] and tomographic images [Zhao *et al.*, 1994; Zhao, 2001], the thickness of the subducting plate is fixed to be 85 km. Both the P and S velocity contrasts are set to be 6% at the top and 3% at the bottom of the slab, respectively, compared with the surrounding mantle. Since a thin low-velocity subducting oceanic crust has been commonly observed in most subduction zones, typically beneath the Japan arc [Matsuzawa *et al.*, 1986; Helffrich and Stein, 1993; Abers and Sarker, 1996; Abers, 2000], an 8-km-thick layer, resembling the oceanic crust, is superposed right above the high-velocity slab. The velocity in this layer is assumed to be 6% lower than that of the mantle above. In the mantle wedge area, low velocities and a gradual velocity transition around the Moho of the overriding plate are introduced to simulate the complex structures there. Double discontinuities are built into the model around 250 km depth in consideration of the strong signals observed below the slab (220–270 km depths in Figures 4b and 4c). There is no evidence in the low-frequency images that such double discontinuities exist, but introducing double discontinuities would be useful for discussing the effects of frequency dependency in imaging. The two discontinuities are designed to have varying separation depths and topography. The final model structure is shown in Figure 6a.

[17] Synthetic tests indicate that our data for profile B–B' is adequate to recover the coherent slab image up to ~ 150 km, and the apparent “disappearance” of the slab below about 150 km may be a result of limited data coverage (Figure 6b). The synthetic image constructed using the real data coverage is only able to recover the top 150 km part of the slab (Figure 6b), although the slab is present at much larger depths in the model (Figure 6a). The slab can be coherently imaged in the whole model space if sufficient data are available, although the strength of the slab image appears weaker when the $PpPs$ Moho multiples start to interfere with the slab conversions (Figure 6c). Such a reduction of image strength could be attributed partially to the cancellation of the positive P -to- S converted phase of the slab with the negative $PsPs + PpSs$ Moho multiples and partially to an illumination problem associated with limited acquisition aperture and propagation effects of shallow structures [Xie and Wu, 2002; Wu and Chen, 2005; Chen *et al.*, 2004]. In the latter case, deeper structures usually have weaker images than the shallower ones. While it is also possible that the slab may become seismically invisible at those depths because its crustal velocity structure becomes indistinguishable from the surrounding mantle (due to, for example, eclogitization of the subducting oceanic crust [Ringwood and Green, 1966; Ahrens and Schubert, 1975; Schmidt and Poli, 1998; Peacock and Wang, 1999]), the fact that our synthetic tests could not well recover the slab below 150 km with the current data coverage suggests that the insufficient data coverage may be responsible for the invisible slab image at depths greater than 150 km in the migration profile (Figure 4b).

[18] Under the current data condition, the Moho of the overriding plate can be continuously imaged (except for the mantle wedge area) in the synthetic modeling (Figure 6b), in contrast to the real data case (Figure 4b). The reason for the invisibility of the continent Moho beneath southern NE

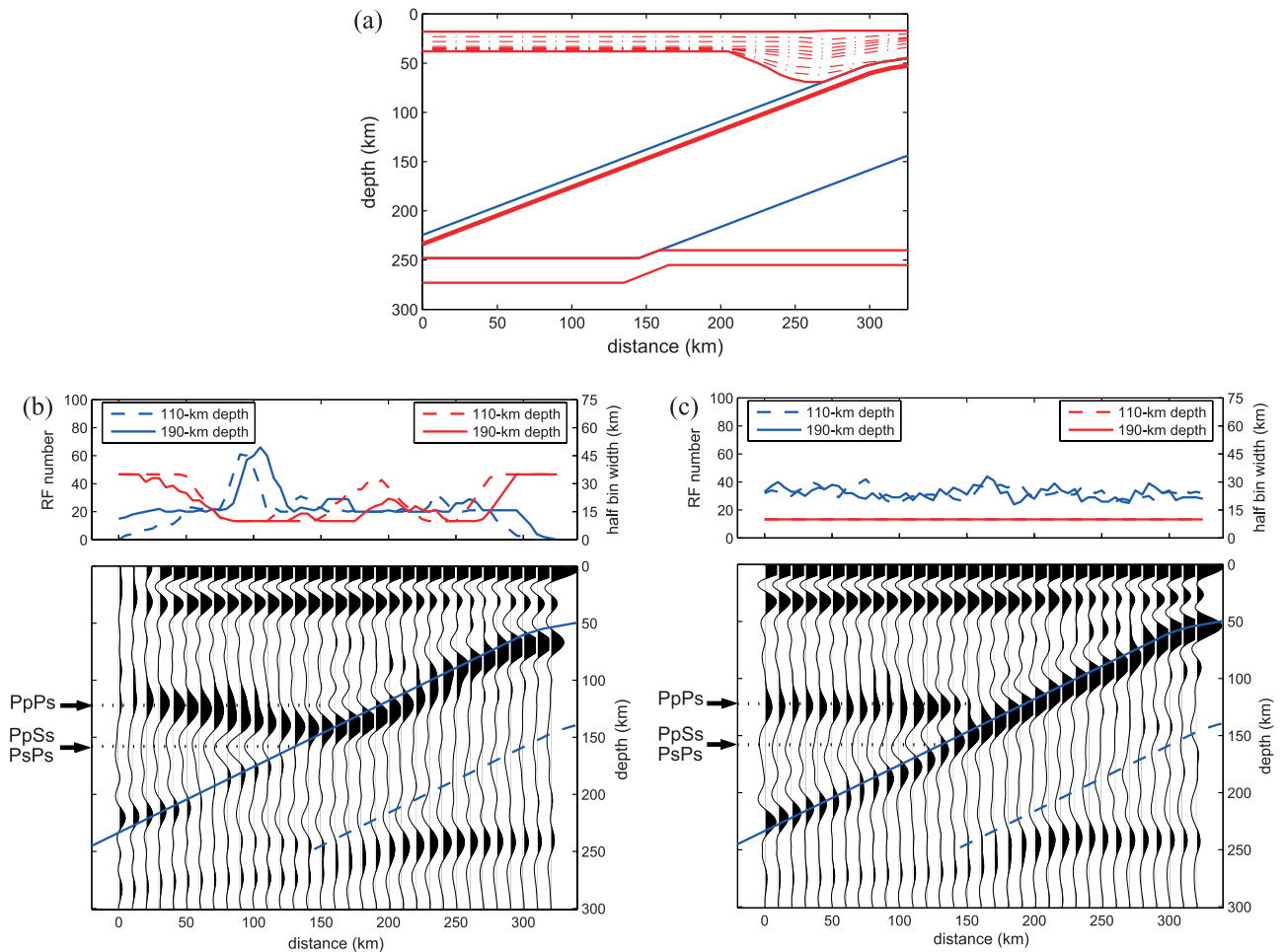


Figure 6. (a) Synthetic subduction zone model constructed on the basis of the migrated image of profile B-B'. Red lines mark discontinuities from a low velocity to a high one, and blue lines denote those from high to low velocities. The thick red line represents the subducting oceanic Moho. Dashed lines denote interfaces with relatively small velocity contrasts. (b and c) Migrated images for the synthetic model based on the real data distribution (Figure 6b) and dense spatial distribution (Figure 6c). The migrated images are constructed using the same frequency contents as in the data images in Figure 4b. Blue lines mark Moho (solid) and lower boundary (dashed) of the descending slab, and black dotted lines mark Moho multiples of the overriding plate.

Japan in the data image is unclear. It may be caused by either a gradual velocity transition between the crust and upper mantle or existence of small-scale topography that destroys the stacking coherency of the limited number of receiver functions. Both of them, however, are unlikely to produce Moho multiples as strong as that presented at ~ 150 km depth in the migrated image (Figure 4b). More plausibly, the indiscernibility of the Moho conversion might be attributed to specific unknown shallow structures (e.g., broadly distributed sedimentary cover). Such structures tend to exert substantial influence on the image of the Moho, but have less effect on deeper structures and multiple induced artifacts (see also examples in Figure 7 in *Chen et al.* [2005]).

[19] With the data available, synthetic tests indicate that the strong signals observed around 250 km depth in the data image are likely real, although it is impossible to distinguish double discontinuities from a single one in the frequency range used in the imaging. The deep seismic discontinuities below the slab are well recovered in the image using the real data sampling (Figure 6b), although the images of the double

discontinuities merge as one even with an ideal data distribution (Figure 6c). The image of the discontinuities displays significant lateral variation in strength, apparently due to the considerable velocity contrast between the slab and the underlying mantle. Such synthetic tests indicate that the similar feature observed in the real data image (Figure 4b) does not reflect change of strength of the discontinuity (or discontinuities), it is rather a characteristic of an imaged discontinuity beneath a structurally complex subduction zone.

[20] For profile C-C', a simple subduction zone model is designed to test whether the shallow breakdown of the slab image (Figure 5b) is real or just a result of insufficient data. The model consists of a two-layer descending plate with a dipping angle of 20° and an undulating Moho of the overriding plate at around 32 km depth (Figure 7a).

[21] Synthetic result demonstrates that the shallow "breakdown" of the real data image (Figure 5b) is unlikely caused by the insufficient data coverage, but more possibly reflects that the slab becomes seismically invisible at depths larger than 60 km. The real data distribution for profile C-C'

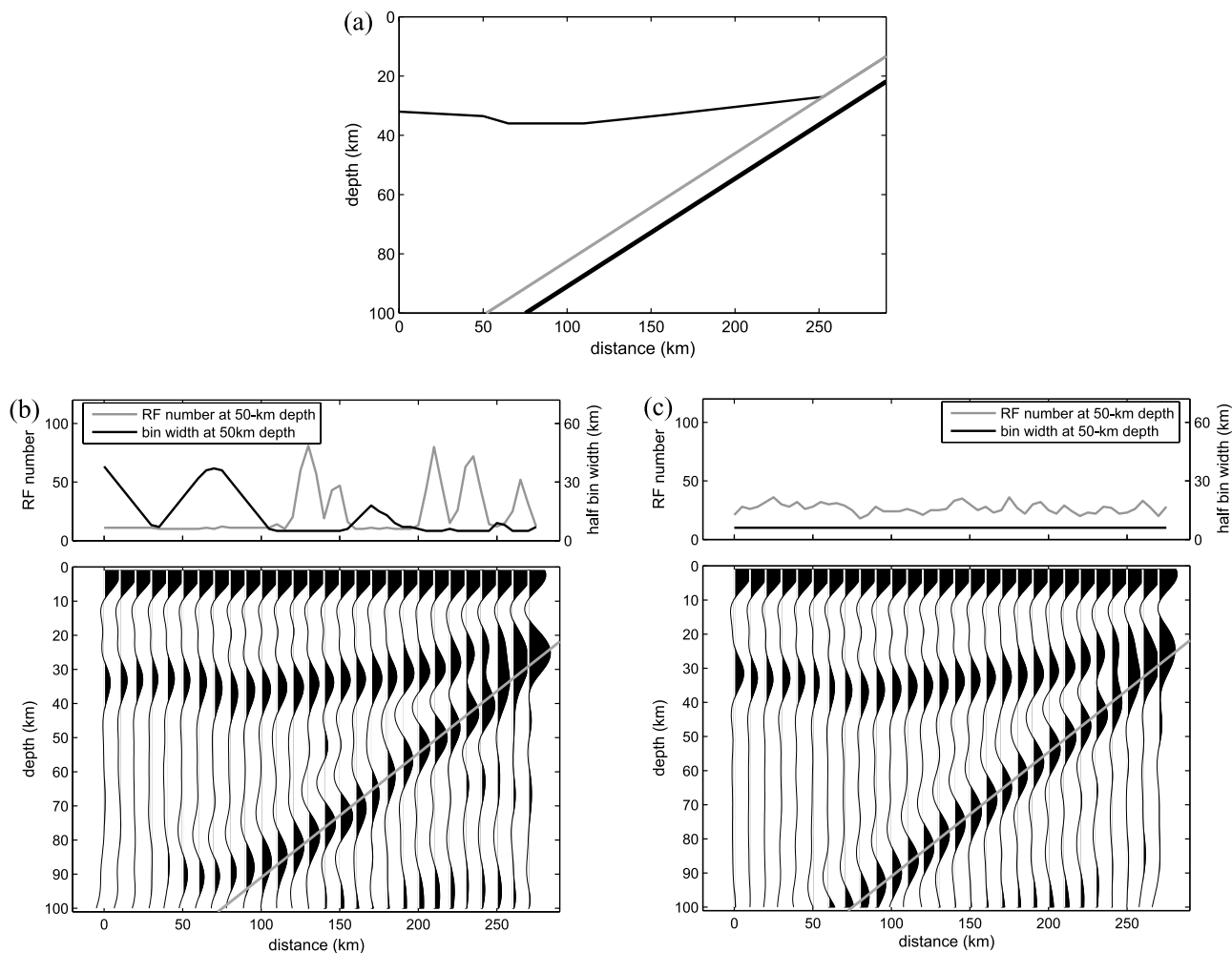


Figure 7. Same as Figure 6, except for profile C-C' and the migrated images (Figures 7b and 7c) are constructed using the same frequency contents as in Figure 5b.

would have enabled us to continuously detect a descending slab to a depth of ~ 90 km, if it were truly discernible from the surrounding mantle (Figure 7b). Expanded data coverage improves the slab image, but only below 90 km depth (Figure 7c).

4.2. Frequency Contributions

[22] In real data application, cutoff frequencies would also need to be chosen in consideration of noise, data distribution, and structural complexities. We have adopted cutoff frequencies of 0.03–0.3 Hz for profiles A-A' and B-B' and 0.03–0.5 Hz for profile C-C'. As we mention in the companion paper, the required data frequencies usually decrease as the depth of the target structures increases. So, relatively higher frequency contributions are used in the construction of the image of the Philippine Sea plate (Figure 5b), which descends at much shallower depths in SW Japan compared with the Pacific plate in NE Japan (Figures 3b and 4b). Because of the low frequencies used in the migration process, our images have limited resolutions in revealing fine structures within the slab. Most noticeably, a thin low-velocity oceanic crust cannot be convincingly identified in the migrated images of profiles A-A' and B-B' (Figures 3b and 4b). This is due to the low cutoff frequencies adopted in imaging. A thin low-velocity oceanic crust

would produce a converted phase with a negative polarity, which is hardly distinguishable from the wavelet of the positive *P*-to-*S* converted phase of the slab in the low-frequency images (Figures 3b and 4b). Synthetic tests indicate that, to resolve a thin low-velocity layer with a thickness of 8 km or the double discontinuities around 250 km in the synthetic model in Figure 6a, a cutoff frequency of 0.6 Hz or higher is required in imaging. Note that distinct negative pulses above the slab images are clearly identifiable in the migrated images of the synthetics, so are the double discontinuities around 250 km depth (Figures 8a and 8b). The high-frequency data images seem to show more details of possible structural features. For example, a clear negative phase appears at 60–120 km depth right above the subducting Pacific plate in the images with cutoff frequency of 0.6 Hz and 1.0 Hz (Figures 8c and 8d), possibly representative of the upper boundary of a thin low-velocity oceanic crust. The strong signals observed in the lower-frequency image around 250 km appear to be two split phases, more likely characteristic of a structure of double discontinuities rather than one discontinuity. With increased frequencies, negative phases are more pronounced in the mantle wedge, possibly indicating the existence of low-velocity zones associated with partial melt induced by slab dehydration in the NE Japan subduction zone

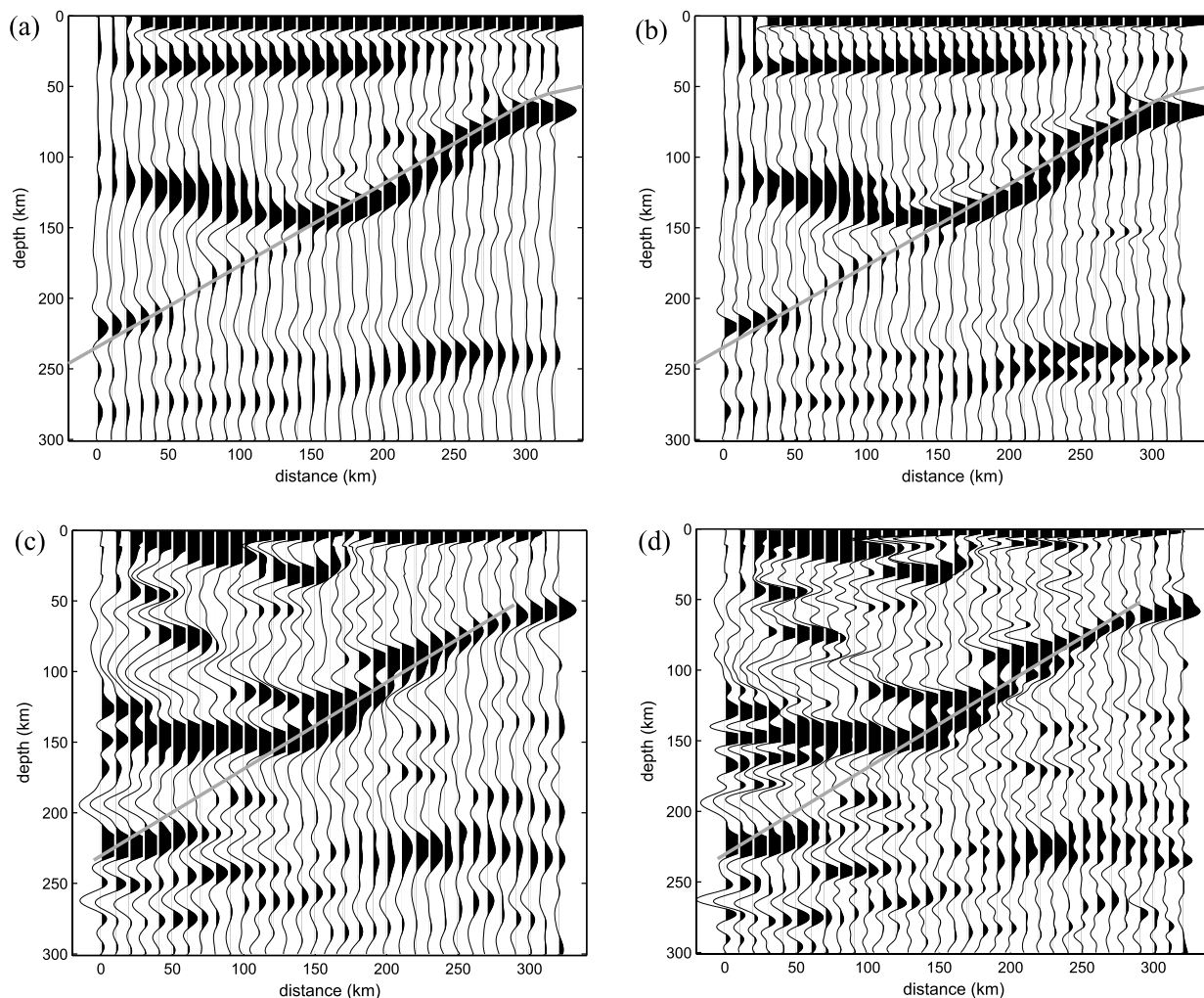


Figure 8. Migrated images (a, b) for the subduction zone model shown in Figure 6a and (c, d) from real data for profile B-B' obtained by using different frequency contributions of receiver functions: 0.03–0.6 Hz (Figures 8a and 8c) and 0.03–1.0 Hz (Figures 8b and 8d). Subducted oceanic Moho in the synthetic model and that estimated from the data image are marked as thick gray lines.

[Hirahara *et al.*, 1989; Schmidt and Poli, 1998; Zhao *et al.*, 2002].

[23] The above interpretations of the high-frequency images, however, still require caution. High-frequency images have the potential of revealing fine structural features. They are, however, also more likely contaminated with various noise-induced artifacts. High-frequency images would require existence of structurally coherent features within the stacking bins up to smaller scales to effectively amplify the signal, and a large number of receiver functions in the stacking to effectively suppress the data noise. While it is possible that our high-frequency images may have suggested the existence of small-scale structures we discuss above, the migrated slab images also appear to be distorted in places, likely reflecting the insufficient coverage of the data and/or incoherency of structural features within the stacking bins. Given the data coverage we have, we choose to interpret the images only up to 0.3 Hz.

4.3. Lateral Seismic Heterogeneities

[24] Up to now, we have used the 1-D PREM to construct the receiver function images for the Japan subduction zone,

since no generally recognized 3-D reference model for the study region is currently available to us. Obviously, the depth distribution of the slab image depends on the velocity structures of the overlying mantle wedge and the continental crust. It has been recognized that slower velocities are typically present in mantle wedges [Zhao *et al.*, 1995; Zhao, 2001], and significant lateral heterogeneities are reported for the crustal structure at various plate boundaries [Zhao *et al.*, 1992a; Christeson *et al.*, 1999; Nakajima *et al.*, 2001, 2002; Takahashi *et al.*, 2002; DESERT Group *et al.*, 2004]. Therefore alternative 2-D velocity models may need to be investigated in the migration process.

[25] We adopt two types of velocity models to re-image the subducting slab for profile B-B' to investigate the influence of lateral heterogeneity on the migrated images. One is designed to simulate the effect of a low-velocity mantle wedge (model X) and the other to study the effect of complex crustal structures. Model X is designed based on the delineated slab geometry in Figure 4b and the results from a *P* wave tomographic model by Zhao *et al.* [1994]. The model is separated into upper and lower portions by the dipping oceanic Moho, and an additional 8-km-thick low-

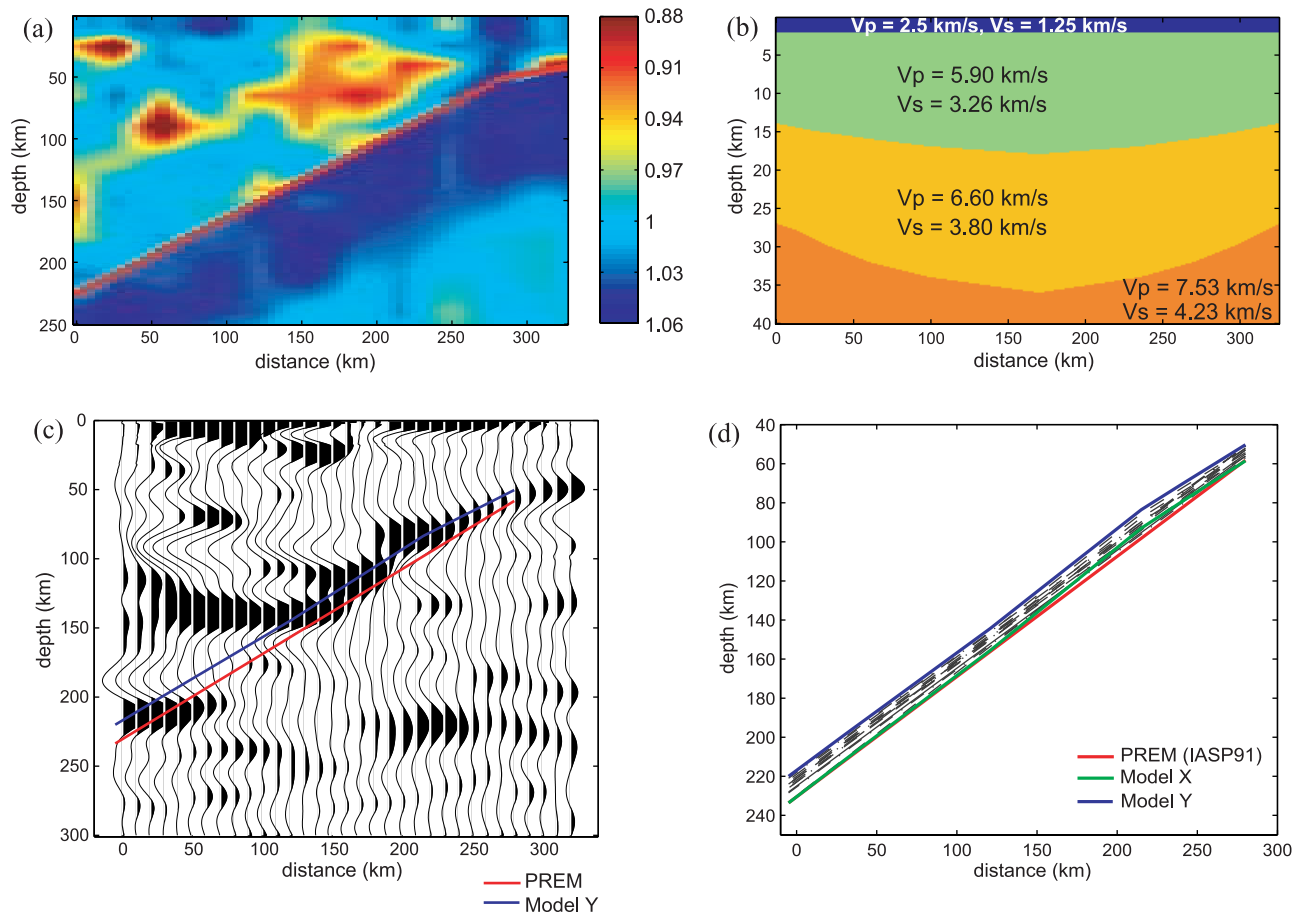


Figure 9. Sensitivity of the migrated images to seismic velocity structures for profile B-B'. (a) Model X in terms of migration velocity (correlated with P and S wave velocities, V_p and V_s , by equation (13) of Chen *et al.* [2005]) with respect to the PREM. V_p model is from the tomographic result by Zhao *et al.* [1994]. V_s is assumed to have the same perturbations as V_p below the slab and 2 times that of V_p in the mantle wedge. (b) Crustal structure of model Y. All the V_p and V_s except the V_s in the upper crust and both velocities in the basin are similar as those given by Zhao *et al.* [1992b]. The depth distributions of the Conrad and the Moho discontinuities are also designed according to those determined by Zhao *et al.* [1992b]. The V_s in the upper crust, obtained with a same V_p/V_s ratio as that of the PREM, is much lowered than that in Zhao *et al.*'s study (3.5 km/s) to enlarge the whole migration velocity difference above the slab between model Y and the PREM. V_p in the 2-km-thick basin is from Figure 4 of Hasegawa *et al.* [1994], and a V_p/V_s ratio of 2 is used to give the V_s there. Below 40-km depth, model Y is same as model X. (c) Poststack-migrated image using model Y with a same frequency range as in Figures 3b and 4b. Red line and blue line give the locations of the oceanic Moho estimated using the PREM and model Y, respectively. (d) Comparison of the estimated Moho locations of the subducting Pacific slab using different velocity models. Black dashed lines are obtained using various 2-D velocity models other than models X and Y.

velocity layer is sandwiched between the two portions, representing the subducting oceanic crust (Figure 9a). Background P velocity perturbations are from the tomography result by Zhao *et al.* [1994]. S velocity perturbations are assumed to be the same as the P velocity perturbations below the slab and 2 times the P velocity perturbations in the mantle wedge. The high V_p/V_s ratio in the mantle wedge is invoked to account for the higher sensitivity of S velocity to the presence of fluids or melts [Hacker *et al.*, 2003a; Goes *et al.*, 2000]. Second type of models involve different crustal models of the overriding plate that are superposed to the above model, including the P wave velocity model given in Figure 4 of Hasegawa *et al.* [1994] for the Honshu area, the crustal

velocity structure derived by Zhao *et al.* [1992a], the one adopted by Nakajima *et al.* [2002] for the central part of NE Japan, and some others with modified crustal velocities, stratifications and Moho shapes. One of the resultant crustal velocity models (model Y) and the corresponding migrated image are shown as an example in Figures 9b and 9c, respectively. The 1-D IASP91 global model [Kennett and Engdahl, 1991] is also tested in comparison with PREM.

[26] Little difference is detected between the images using IASP91 and PREM as migration velocity model (Figure 4b). The imaged structural features obtained by incorporating the substantial lateral velocity variations above the slab into migration velocity model are not significantly different from

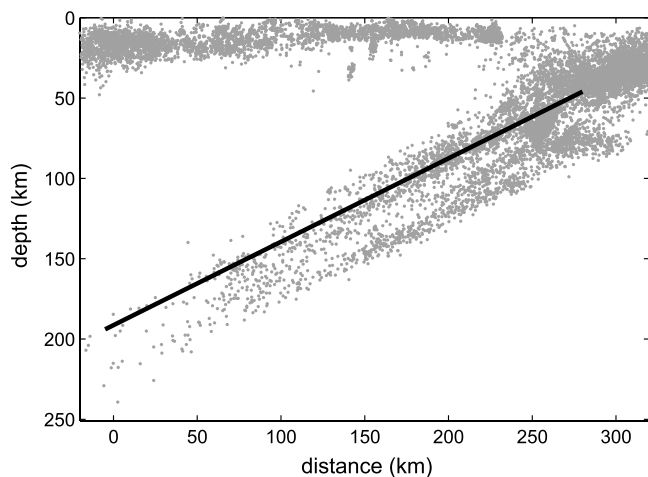


Figure 10. Comparison of the imaged oceanic Moho location (black line) for profile A-A' with the hypocenter loci of earthquakes of magnitude 1.0 and above (gray dots) occurring within the corresponding stacking area (rectangular area in Figure 1) from June 2002 to June 2004.

that presented in the image using PREM or IASP91 as the migration velocity model (compare Figure 9c with Figure 4b). The estimated Moho of the slab is only slightly curved when adopting model X in migration. It becomes a little convex at 80–90 km depths (see green line in Figure 9d) where the effect of low-velocity anomalies in the mantle wedge is the strongest. On the other hand, models of the overriding continental crust with lowered velocities than PREM tend to influence the image more, making the slab and underlying discontinuities somewhat shallowed (compare blue line with green line in Figure 9d). The combined effect of mantle wedge and continental crust results in a depth-dependent difference in estimated oceanic Moho depth, from ~ 8 km at 50 km depth to ~ 14 km around

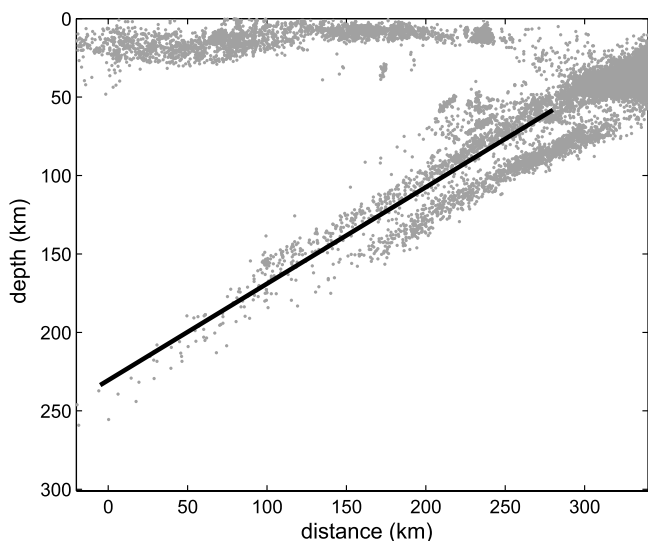


Figure 11. Same as Figure 10 except for profile B-B'.

90 km depth, and a nearly constant fluctuation of 12–14 km below that depth. The estimated dip angles from different velocity models vary only slightly around the PREM-based one (32°) with majorities falling into the $\pm 1^\circ$ range (Figure 9d). Such a small dip angle difference indicates that lateral heterogeneities and different velocity stratifications would not significantly affect slab geometry estimation at 50–200 depths. Nevertheless, more detailed crustal and mantle wedge models are certainly necessary to better constrain the depth distribution of the slab and to improve the accuracy and reliability of the migrated image for fine-scale structures at shallower depths.

5. Spatial Relationship Between Slab and Seismicity

[27] We study the relationships between the geometry of the subducting oceanic Moho inferred from the migrated images (Figures 3b–5b) and the hypocentral loci of earthquakes of magnitude 1.0 and above occurring within each of the block areas (Figures 10–12). The purpose is twofold. We use the seismicity as an independent source to check the validity of the slab geometries inferred from the migrated

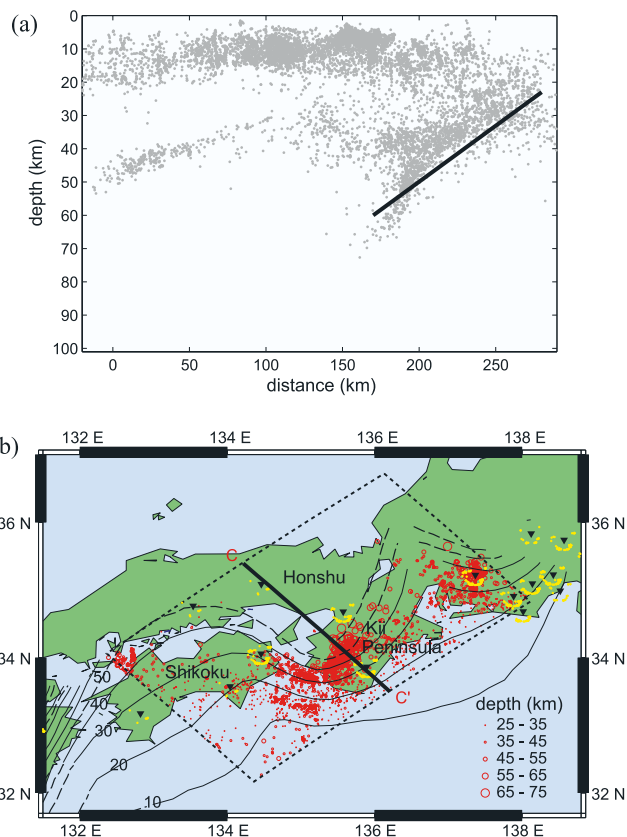


Figure 12. (a) Same as Figure 10 except for profile C-C'. (b) Epicenter distribution of the earthquakes (red circles) within a depth range of 25–80 km. Depth contour lines of the Philippine Sea plate are from Wang *et al.* [2004]. Inverted triangles represent FREESIA broadband stations, and yellow dots denote the piercing points of P-to-S conversion at 50 km depth.

images; we examine the spatial distributions of earthquakes and their relationships to the slab images between the two types of subducting oceanic plates. The seismicity data covers a 2-year period from June 2002 to June 2004 as a part of the Japan University Network Earthquake Catalog collected at the Earthquake Research Institute, University of Tokyo. A 1-D velocity model similar to IASP91 was used for hypocenter determination, which permits us to compare the slab images from PREM (IASP91) with seismicity without significant systematic relocation errors. The hypocenters are projected to the image profiles in the same manner as are the piercing points of *P*-to-*S* converted phases.

[28] The inferred geometries of the imaged Pacific plate are in good agreement with the seismicity pattern beneath NE Japan (Figures 10 and 11). The intermediate-depth earthquakes form a double seismic zone along the two profiles in NE Japan. The seismicity of profile A-A' shows a more scattered distribution than that of profile B-B' (Figures 10 and 11). This may be due to the fact that the earthquake locations are projected over a larger spatial extent in the northern block. The delineated Moho of the subducting slab for profile A-A' is located within the upper seismic plane, 8–15 km beneath its top surface in the depth range of 70–150 km where the slab is clearly imaged. For profile B-B', the obtained location of the Moho is just below the 8- to 10-km-thick upper seismic plane. Assuming that the thickness of the descending oceanic crust is less than 10 km [Matsuzawa *et al.*, 1986; Abers, 2000], the slab geometry obtained from our receiver function analysis indicates that the events in the upper seismic plane mainly occur within the oceanic crust, while those in the lower seismic plane are located in the oceanic lithospheric mantle, agreeing well with previous seismicity and seismological studies [Matsuzawa *et al.*, 1986, 1990; Igarashi *et al.*, 2001].

[29] Both the shape of the descending slab and the seismicity pattern in SW Japan are reported to be more complex [Nakamura *et al.*, 1997; Matsumura, 1997; Ishida, 1992; Goto *et al.*, 2001; Baba *et al.*, 2002; Nakanishi *et al.*, 2002], largely due to the specific subduction history of the Philippine Sea plate [Wang *et al.*, 2004]. Hypocenter data show that most of the deep events in eastern SW Japan occur above the imaged Moho of the slab to a depth of ~60 km. Below that depth, the earthquakes tend to occur in the subducting lithospheric mantle (Figure 12a). This result corroborates with previous seismic observations that most of intraslab events in this region occur in the subducting oceanic crust with maximum depths of ~50–65 km [Nakamura *et al.*, 1997; Ohkura, 2000; Seno *et al.*, 2001]. The estimated slab dip angle of ~19° is also very close to what was previously inferred from seismicity (~20°) [Yamasaki and Seno, 2003]. Note that in addition to the seismic zone with a ~20° dipping angle in the southeastern part of profile C-C', another seismic zone with a shallower dip is clearly present in northwest. Epicenter distribution of earthquakes at 25–80 km depth (Figure 12b) indicates that the former represents the seismicity in and around the Kii Peninsula, while the later is contributed mainly from the events beneath the Shikoku island and further north where the Philippine Sea plate descends at a dip angle of about 10° [Shiomi *et al.*, 2004]. The shallow subduction and the fact that few data are available in this area, however,

make the Moho of the oceanic plate barely discernible (Figures 5b and 5c).

[30] The contrasting features of both the slab images and intraslab seismicity between the relative young Philippine Sea plate and the old Pacific plate may be attributed to the large temperature difference between the two plates, which may result in different depth and nature of dehydration reactions in the two subducting slabs. Dehydration reactions within a slab play an important role in influencing the seismic velocity structure and the seismicity pattern in a subduction zone [Peacock and Wang, 1999; Julian, 2002; Yamasaki and Seno, 2003]. The completion of the dehydration induced gabbro or blueschist to eclogite transformation in the hydrated subducting oceanic crust [Ringwood and Green, 1966; Ahrens and Schubert, 1975; Schmidt and Poli, 1998] would make the subducting oceanic Moho invisible to the *P*-to-*S* converted phases, since anhydrous eclogite cannot be distinguished from the surrounding mantle on the basis of wave speeds [Helffrich *et al.*, 1989; Sobolev and Babeyko, 1994; Hacker *et al.*, 2003a]. Dehydration reactions in the subducting slabs is also proposed as a plausible process triggering intermediate-depth intraslab earthquakes [Green and Houston, 1995; Kirby, 1995; Kirby *et al.*, 1996]. Seismological evidences suggest that the hydrated rocks in the subducting crust at the Nankai margin persist to ~60 km depth [Hori *et al.*, 1985; Ohkura, 2000], and the thermal structure constructed by Hacker *et al.* [2003b] for the slab under the Kii Peninsula further indicates a complete eclogitization of the hydrated minerals at ~80 km. Our receiver function image (Figure 5b) therefore supports the dehydration reaction interpretation for the invisibility of the subducting Philippine Sea plate at shallower depths and the lack of deep intraslab seismicity in SW Japan. The descending Pacific plate in NE Japan, on the other hand, remains visible to at least 150 km depth in our receiver function image (Figure 4b), consistent with body wave dispersion observations that suggest that eclogite is not an important part of the subducting crust down to 100–250 km [Abers, 2000]. The greater detectable depths of the subducting oceanic Moho and deep extent of intraslab earthquakes are largely attributed to the persistence of hydrated phases in depth and kinetically delayed eclogitization due to the much lower temperature of the Pacific plate [Peacock and Wang, 1999]. Abrupt breakdown of a slab has also been observed along with the termination of intermediate-depth seismicity by Yuan *et al.* [2000] in their receiver function image for the subducted Nazca plate beneath central Andes [Yuan *et al.*, 2000]. The 120 km depth at which the slab image disappeared lies between those for the Pacific plate in NE Japan and the Philippine Sea plate in SW Japan, concordant with the depths of complete oceanic crust eclogitization estimated based on the predicted thermal structure of these subducting plates [Peacock and Wang, 1999; Stern, 2002; Yamasaki and Seno, 2003]. This indicates that the dehydration induced eclogitization mechanism may be appropriate for explaining the observations for all the three subducting plates.

6. Conclusions

[31] The wave equation based poststack migration method for receiver function imaging is applied to the real

data set collected at the broadband seismic stations in Japan and demonstrates its ability to image the dipping slabs of different types. With the data currently available to us, the subducting Pacific plate in NE Japan and the Philippine Sea plate in the eastern part of SW Japan are coherently imaged. The migrated oceanic Moho images of the Pacific plate extend down to ~ 150 km depth with a dip angle of $\sim 30^\circ$ then disappear at larger depths. The imaged Philippine Sea plate exhibits a shallow subduction of $\sim 19^\circ$ and is clearly detected only within a depth range of 25–60 km. Synthetic experiments indicate that, under the current data condition, the inferred structural features of the slab images are well resolved in the top 150 km for the Pacific plate and top 80 km for the Philippine sea plate. The “disappearance” of the Pacific plate below 150 km in the migration images is likely a result of insufficient data, while the invisibility of the Philippine Sea plate at depths larger than ~ 60 km is a real, well-resolved, feature.

[32] Comparisons between migrated and CCP stacked images demonstrate the advantages of the migration method over the CCP stacking technique in imaging complex subsurface structures. The migration procedure produces more coherent slab images with higher SNR, as a consequence of proper handling of the propagation effects of lateral heterogeneities through wave field extrapolation. Synthetic tests also indicate that our images are not affected much by lateral heterogeneities in the mantle wedge or in the continental crust. With improved data density and coverage, the migration method could potentially resolve the slab images below 150 km for the Pacific plate and fine-scale structures in high-frequency imaging.

[33] The imaged slab geometries coincide with the spatial distributions of intermediate-depth earthquakes beneath NE and SW Japan, confirming the validity of the migration technique in imaging the complex structures. The estimated Moho of the Pacific plate is located near the bottom of the upper plane of the observed double seismic zones, while that of the Philippine plate is below most of deep events. The depth extent of the seismicity appears to correlate with the depth extent of the slab images between the two subduction zones, with the Pacific plate extending to ~ 150 km and possibly deeper and the Philippine Sea plate only to ~ 60 km. The contrasting image features along with their correlated distinct seismicity patterns between the relative young Philippine Sea plate and the old Pacific plate may be attributed to the large temperature difference between the two plates, which may result in different depth and nature of dehydration reactions in the two subducting slabs.

[34] **Acknowledgments.** We wish to thank the FREESIA project for providing the waveform data, Xiaohui Yuan, an anonymous reviewer, and Associate Editor for thoughtful reviews. We are especially grateful to Fenglin Niu for assisting the waveform data collection and Zhao Dapeng and Mohamed Farouk for collecting and providing the hypocenter data from the Japan University Network Earthquake Catalog. This research has been supported by the National Science Foundation of China (grants 40434012 and 40374015), the Chinese Academy of Sciences, and NSF grant 0309859.

References

Abers, G. A. (2000), Hydrated subducted crust at 100–250 km depth, *Earth Planet. Sci. Lett.*, *176*, 323–330.

- Abers, G. A., and G. Sarker (1996), Dispersion of regional body waves at 100–150 km depth beneath Alaska: In situ constraints on metamorphism of subducted crust, *Geophys. Res. Lett.*, *23*, 1171–1174.
- Ahrens, T. J., and G. Schubert (1975), Gabbro-eclogite reaction rate and its geophysical significance, *Rev. Geophys.*, *13*, 383–400.
- Ai, Y., T. Zheng, W. Xu, Y. He, and D. Dong (2003), A complex 660 km discontinuity beneath northeast China, *Earth Planet. Sci. Lett.*, *212*, 63–71.
- Baba, T., Y. Tanioka, P. R. Cummins, and K. Uehira (2002), The slip distribution of the 1946 Nankai earthquake estimated from tsunami inversion using a new place model, *Phys. Earth Planet. Inter.*, *132*, 59–73.
- Bostock, M., and S. Rondenay (1999), Migration of scattered teleseismic body waves, *Geophys. J. Int.*, *137*, 732–746.
- Bostock, M., S. Rondenay, and J. Shragge (2001), Multiparameter two-dimensional inversion of scattered teleseismic body waves: 1. Theory for oblique incidence, *J. Geophys. Res.*, *106*, 30,785–30,796.
- Chen, L., R. S. Wu, and W. Wang (2004), Common angle image gathers obtained from Gabor-Daubechies beamlet prestack depth migration (in both Chinese and English), *Chin. J. Geophys.*, *47*, 876–885.
- Chen, L., L. Wen, and T. Zheng (2005), A wave equation migration method for receiver function imaging: 1. Theory, *J. Geophys. Res.*, *110*, B11309, doi:10.1029/2005JB003665.
- Christeson, G. L., K. D. McIntosh, and T. H. Shipley (1999), Structure of the Costa Rica convergent margin, offshore Nicoya Peninsula, *J. Geophys. Res.*, *104*, 25,443–25,468.
- DESERT Group, et al. (2004), The crustal structure of the Dead Sea Transform, *Geophys. J. Int.*, *156*, 655–681.
- Dueker, K. G., and A. F. Sheehan (1997), Mantle discontinuity structure from midpoint stacks of converted *P* to *S* waves across the Yellowstone hotspot track, *J. Geophys. Res.*, *102*, 8313–8327.
- Dziewonski, A., and D. L. Anderson (1981), Preliminary reference Earth model, *Phys. Earth Planet. Inter.*, *25*, 297–356.
- Gilbert, H. J., A. F. Sheehan, K. G. Dueker, and P. Molnar (2003), Receiver functions in the western United States, with implications for upper mantle structure and dynamics, *J. Geophys. Res.*, *108*(B5), 2229, doi:10.1029/2001JB001194.
- Goes, S., R. Govers, and P. Vacher (2000), Shallow mantle temperatures under Europe from *P* and *S* wave tomography, *J. Geophys. Res.*, *105*, 11,153–11,169.
- Goto, K., T. Honda, H. Yakiwara, T. Kakuta, and H. Shimizu (2001), Geometry and focal mechanisms of moderately deep seismic zone beneath southern Kyushu (in Japanese), *Chikyū Mon.*, *23*, 664–668.
- Green, H. W., and H. Houston (1995), The mechanics of deep earthquakes, *Annu. Rev. Earth.*, 169–213.
- Gudmundsson, O., and M. Sambridge (1998), A regionalized upper mantle (RUM) seismic model, *J. Geophys. Res.*, *103*, 7121–7136.
- Hacker, B. R., G. A. Abers, and S. M. Peacock (2003a), Subduction factory, 1. Theoretical mineralogy, density, seismic wave speeds, and H_2O content, *J. Geophys. Res.*, *108*(B1), 2029, doi:10.1029/2001JB001127.
- Hacker, B. R., S. M. Peacock, G. A. Abers, and S. D. Hollaway (2003b), Subduction factory: 2. Are intermediate-depth earthquakes in subducting slabs linked to metamorphic dehydration reactions?, *J. Geophys. Res.*, *108*(B1), 2030, doi:10.1029/2001JB001129.
- Hasegawa, A., N. Umino, and A. Takagi (1978), Double-planed deep seismic zone and upper mantle structure in the northeastern Japan arc, *Geophys. J. R. Astron. Soc.*, *54*, 281–296.
- Hasegawa, A., S. Horiuchi, and N. Umino (1994), Seismic structure of the northeastern Japan convergent margin: A synthesis, *J. Geophys. Res.*, *99*, 22,295–22,311.
- Helfrich, G. R., and S. Stein (1993), Study of the structure of the slab-mantle interface using reflected and converted seismic waves, *Geophys. J. Int.*, *115*, 14–40.
- Helfrich, G. R., S. Stein, and B. J. Wood (1989), Subduction zone thermal structure and mineralogy and their relationship to seismic wave reflections and conversions at the slab/mantle interface, *J. Geophys. Res.*, *94*, 753–763.
- Hirahara, K., A. Ikami, M. Ishida, and T. Mikumo (1989), Three dimensional *P*-wave velocity structure beneath Central Japan: low-velocity bodies in the wedge portion of the upper mantle above high-velocity subducting plate, *Tectonophysics*, *163*, 63–73.
- Hori, S., H. Inoue, Y. Fukao, and M. Ukawa (1985), Seismic detection of the untransformed “basaltic” oceanic crust subducting into the mantle, *Geophys. J. R. Astron. Soc.*, *83*, 169–197.
- Igarashi, T., T. Matsuzawa, N. Umino, and A. Hasegawa (2001), Spatial distribution of focal mechanisms for interplate and intraplate earthquakes associated with the subducting Pacific plate beneath the northeastern Japan arc: A triple-planed deep seismic zone, *J. Geophys. Res.*, *106*, 2177–2191.
- Iidaka, T., M. Mizoue, I. Nakamura, T. Tsukuda, K. Sakai, M. Kobayashi, T. Haneda, and S. Hashimoto (1990), The upper boundary of the Philip-

- pine Sea plate beneath the western Kanto region estimated from *SP* converted waves, *Tectonophysics*, 179, 321–326.
- Ishida, M. (1989), Seismicity and tectonics of Japan, in *Earthquakes and Seismotectonics of the Japanese Islands*, edited by T. Hagiwara, pp. 57–85, Kaijima Inst., Tokyo.
- Ishida, M. (1992), Geometry and relative motion of the Philippine Sea plate and Pacific plate beneath the Kanto-Tokai district, Japan, *J. Geophys. Res.*, 97, 489–513.
- Julian, B. (2002), Seismological detection of slab metamorphism, *Science*, 296, 1625–1626.
- Kennett, B. L. N., and E. R. Engdahl (1991), Travel times for global earthquake location and phase identification, *Geophys. J. Int.*, 105, 429–465.
- Kirby, S. H. (1995), Interslab earthquakes and phase changes in subducting lithosphere, *U.S. Natl. Rep. Int. Union Geod. Geophys. 1991–1994, Rev. Geophys.*, 33, 287–297.
- Kirby, S. H., E. R. Engdahl, and R. Denlinger (1996), Intermediate-depth intraslab earthquakes and arc volcanism as physical expressions of crustal and uppermost mantle metamorphism in subducting slabs, in *Subduction: Top to Bottom, Geophys. Monogr. Ser.*, vol. 96, edited by G. E. Bebout et al., pp. 195–214, AGU, Washington, D. C.
- Langston, C. A. (1977), The effect of planar dipping structure on source and receiver responses for constant ray parameter, *Bull. Seismol. Soc. Am.*, 67, 1029–1050.
- Li, X., S. V. Sobolev, R. Kind, X. Yuan, and C. Estabrook (2000), A detailed receiver function image of the upper mantle discontinuities in the Japan subduction zone, *Earth Planet. Sci. Lett.*, 183, 527–541.
- Matsumura, S. (1997), Focal zone of a future Tokai earthquake inferred from the seismicity pattern around the plate interface, *Tectonophysics*, 273, 271–291.
- Matsuzawa, T., N. Umino, A. Hasegawa, and A. Takagi (1986), Upper mantle velocity structure estimated from PS-converted wave beneath the northeastern Japan arc, *Geophys. J. R. Astron. Soc.*, 86, 767–787.
- Matsuzawa, T., T. Kono, A. Hasegawa, and A. Takagi (1990), Subducting plate boundary beneath northeastern Japan arc estimated from *SP* converted waves, *Tectonophysics*, 181, 123–133.
- Nakajima, J., T. Matsuzawa, A. Hasegawa, and D. Zhao (2001), Seismic imaging of arc magma and fluids under the central part of northeastern Japan, *Tectonophysics*, 341, 1–17.
- Nakajima, J., T. Matsuzawa, and A. Hasegawa (2002), Moho depth variation in the central part of northeastern Japan estimated from reflected and converted waves, *Phys. Earth. Planet. Inter.*, 130, 31–47.
- Nakamura, M., H. Watanabe, T. Konomi, S. Kimura, and K. Miura (1997), Characteristics activities of subcrustal earthquakes along the outer zone of southwestern Japan (in Japanese), *Annu. Disaster Prevent. Res. Inst.*, 40, 1–20.
- Nakanishi, A., et al. (2002), Deep crustal structure of the eastern Nankai trough and the Zenisu Ridge by a dense airgun-OBS seismic profiling, *Mar. Geol.*, 187, 47–62.
- Nakanishi, I. (1980), Precursors to ScS phases and dipping interface in the upper mantle beneath southwestern Japan, *Tectonophysics*, 69, 1–35.
- Nakanishi, I., K. Suyehiro, and T. Yokota (1981), Regional variations of amplitudes of ScSp phases observed in the Japanese Islands, *Geophys. J. R. Astron. Soc.*, 67, 615–634.
- Ohkura, T. (2000), Structure of the upper part of the Philippine Sea plate estimated by later phases of upper mantle earthquakes in and around Shikoku, Japan, *Tectonophysics*, 321, 17–35.
- Okubo, Y., H. Tsu, and K. Ogawa (1989), Estimation of Curie point temperature and geothermal structure of island arcs of Japan, *Tectonophysics*, 159, 279–290.
- Owens, T. J., S. R. Taylor, and G. Zandt (1987), Crustal structure at regional test network stations determined from inversion of broadband teleseismic *P* waveforms, *Bull. Seismol. Soc. Am.*, 77, 631–662.
- Peacock, S. M., and K. Wang (1999), Seismic consequences of warm versus cool subduction zone metamorphism: Examples from northeast and southwest Japan, *Science*, 286, 937–939.
- Poppeliers, C., and G. L. Pavlis (2003a), Three-dimensional, prestack, plane wave migration of teleseismic *P*-to-*S* converted phases: 1. Theory, *J. Geophys. Res.*, 108(B2), 2112, doi:10.1029/2001JB000216.
- Poppeliers, C., and G. L. Pavlis (2003b), Three-dimensional, prestack, plane wave migration of teleseismic *P*-to-*S* converted phases: 2. Stacking multiple events, *J. Geophys. Res.*, 108(B5), 2267, doi:10.1029/2001JB001583.
- Ringwood, A. E., and D. H. Green (1966), An experimental investigation of the gabbro-eclogite transformation and some geophysical implications, *Tectonophysics*, 3, 383–427.
- Rondenay, S., M. G. Bostock, and J. Shragge (2001), Multiparameter two-dimensional inversion of scattered teleseismic body waves: 3. Application to the Cascadia 1993 data set, *J. Geophys. Res.*, 106, 30,795–30,807.
- Ryberg, T., and M. Weber (2000), Receiver function arrays: a reflection seismic approach, *Geophys. J. Int.*, 141, 1–11.
- Schmidt, M. W., and S. Poli (1998), Experimentally based water budgets for dehydrating slabs and consequences for arc magma generation, *Earth Planet. Sci. Lett.*, 163, 361–379.
- Seno, T., S. Stein, and A. Gripp (1993), A model for the motion of the Philippine Sea plate consistent with NUVEL-1 and geological data, *J. Geophys. Res.*, 98, 17,941–17,948.
- Seno, T., T. Sakurai, and S. Stein (1996), Can the Okhotsk plate be discriminated from the North American plate?, *J. Geophys. Res.*, 101, 17,305–11,315.
- Seno, T., D. Zhao, Y. Kobayashi, and M. Nakamura (2001), Dehydration of serpentinized slab mantle: Seismic evidence from southwest Japan, *Earth Planets Space*, 53, 861–871.
- Sheehan, A. F., G. A. Abers, C. H. Jones, and A. L. Lerner-Lam (1995), Crustal thickness variations across the Colorado Rocky Mountains from teleseismic receiver functions, *J. Geophys. Res.*, 100, 20,391–20,404.
- Sheehan, A. F., P. M. Shearer, H. J. Gilbert, and K. G. Ducker (2000), Seismic migration processing of *P-SV* converted phases for mantle discontinuity structure beneath the Snake River Plain, western United States, *J. Geophys. Res.*, 105, 19,055–19,065.
- Shiomi, K., H. Sato, K. Obara, and M. Ohtake (2004), Configuration of subducting Philippine Sea plate beneath southwest Japan revealed from receiver function analysis based on the multivariate autoregressive model, *J. Geophys. Res.*, 109, B04308, doi:10.1029/2003JB002774.
- Shragge, J., M. G. Bostock, and S. Rondenay (2001), Multiparameter two-dimensional inversion of scattered teleseismic body waves: 2. Numerical examples, *J. Geophys. Res.*, 106, 30,783–30,793.
- Sobolev, S. V., and A. Y. Babeyko (1994), Modelling of mineralogical composition, density and elastic wave velocities in the unhydrous rocks, *Surv. Geophys.*, 15, 515–544.
- Stern, R. J. (2002), Subduction zones, *Rev. Geophys.*, 40(4), 1012, doi:10.1029/2001RG000108.
- Takahashi, N., et al. (2002), Seismic structure of western end of the Nankai trough seismogenic zone, *J. Geophys. Res.*, 107(B10), 2212, doi:10.1029/2000JB000121.
- Umino, N. (1988), Characteristics of the microseismic activity and seismotectonics in the northeastern Japan arc (in Japanese), thesis, 211 pp., Tohoku Univ., Sendai, Japan.
- Umino, N., and A. Hasegawa (1993), Location of deep earthquakes within the subducted Pacific plate estimated from converted waves, paper presented at Japanese Earth Planetary Science Joint Meeting, *Geod. Soc. of Jpn.*, Tokyo.
- Umino, N., A. Hasegawa, and T. Matsuzawa (1995), *sP* depth phase at small epicentral distances and estimated subducting plate boundary, *Geophys. J. Int.*, 120, 356–366.
- Vinnik, L. P. (1977), Detection of waves converted from *P* to *SV* in the mantle, *Phys. Earth. Planet. Inter.*, 15, 294–303.
- Wang, K., I. Wada, and Y. Ishikawa (2004), Stresses in the subducting slab beneath southwest Japan and relation with plate geometry, tectonic forces, slab dehydration, and damaging earthquakes, *J. Geophys. Res.*, 109, B08304, doi:10.1029/2003JB002888.
- Watanabe, T., M. G. Langseth, and R. N. Anderson (1977), Heat flow in back-arc basins of the western Pacific, in *Island Arcs, Deep Sea Trenches and Back-Arc Basins, Maurice Ewing Ser.*, vol. 1, edited by M. Talwani and W. C. Pitman III, pp. 137–161, AGU, Washington, D. C.
- Wen, L., and D. V. Helmberger (1998), A two-dimensional *P-SV* hybrid method and its application to modeling localized structures near the core-mantle boundary, *J. Geophys. Res.*, 103, 17,901–17,918.
- Wu, Q., and R. Zeng (1998), The crustal structure of Qinghai-Xizang plateau inferred from broadband teleseismic waveform (in Chinese), *Chin. J. Geophys.*, 41, 669–679.
- Wu, R. S., and L. Chen (2005), Mapping directional illumination and acquisition dip response using beamlet decomposition and propagation, *Geophysics*, in press.
- Xie, X. B., and R. S. Wu (2002), Extracting angle domain information from migrated wavefield, 70th Annual International Meeting, Soc. of Expl. Geophys.
- Yamasaki, T., and T. Seno (2003), Double seismic zone and dehydration embrittlement of the subducting slab, *J. Geophys. Res.*, 108(B4), 2212, doi:10.1029/2002JB001918.
- Yuan, X., et al. (2000), Subduction and collision processes in the central Andes constrained by converted seismic phases, *Nature*, 408, 958–961.
- Yuhara, K. (1973), Effect of the hydrothermal systems of the terrestrial heat flow, *Bull. Volcanol. Soc. Jpn.*, 18, 129–142.
- Zhao, D. (2001), Seismological structure of subduction zones and its implications for arc magmatism and dynamics, *Phys. Earth. Planet. Inter.*, 127, 197–214.
- Zhao, D., S. Horiuchi, and A. Hasegawa (1992a), Seismic velocity structure of the crust beneath the Japan Islands, *Tectonophysics*, 212, 289–301.

- Zhao, D., A. Hasegawa, and S. Horiuchi (1992b), Tomographic imaging of *P* and *S* wave velocity structure beneath northeastern Japan, *J. Geophys. Res.*, *97*, 19,909–19,928.
- Zhao, D., A. Hasegawa, and H. Kanamori (1994), Deep structure of Japan subduction zone as derived from local, regional, and teleseismic events, *J. Geophys. Res.*, *99*, 22,313–22,329.
- Zhao, D., D. Christensen, and H. Pulpan (1995), Tomographic imaging of the Alaska subduction zone, *J. Geophys. Res.*, *100*, 6487–6504.
- Zhao, D., T. Matsuzawa, and A. Hasegawa (1997), Morphology of the subducting slab boundary in the northeastern Japan arc, *Phys. Earth Planet. Inter.*, *102*, 89–104.
- Zhao, D., O. P. Mishra, and R. Sanda (2002), Influence of fluids and magma on earthquakes: seismological evidence, *Phys. Earth Planet. Inter.*, *132*, 249–267.
- Zhu, L. (2000), Crustal structure across the San Andreas Fault, southern California from teleseismic converted waves, *Earth Planet. Sci. Lett.*, *179*, 183–190.
-
- L. Chen and T. Zheng, Seismological Laboratory, Institute of Geology and Geophysics, Chinese Academy of Sciences, Beijing 100029, China. (lchen@mail.iggcas.ac.cn)
- L. Wen, Department of Geosciences, State University of New York at Stony Brook, Stony Brook, NY 11794, USA.